Spinon excitations in the quasi-one-dimensional $S = \frac{1}{2}$ chain compound $Cs_4CuSb_2Cl_{12}$

Thao T. Tran,[1,2] Chris A. Pocs,[3] Yubo Zhang,[4,5] Michal J. Winiarski,[1,6] Jianwei Sun,[4] Minhyea Lee,[3] and Tyrel M. McQueen[1,7,*]

[1]*Department of Chemistry, Department of Physics and Astronomy, Institute for Quantum Matter, Johns Hopkins University, Baltimore, Maryland 21218, USA*

[2]*Department of Chemistry, Clemson University, Clemson, South Carolina 29634, USA*

[3]*Department of Physics, University of Colorado at Boulder, Boulder, Colorado 80309, USA*

[4]*Department of Physics and Engineering Physics, Tulane University, New Orleans, Louisiana 70118, USA*

[5]*Department of Physics, Southern University of Science and Technology of China, Shenzhen 518055, China*

[6]*Faculty of Applied Physics and Mathematics, Advanced Materials Center, Gdansk University of Technology, Narutowicza 11/12, 80-233 Gdansk, Poland*

[7]*Department of Materials Science and Engineering, Johns Hopkins University, Baltimore, Maryland 21218, USA*

(Received 6 February 2020; revised manuscript received 30 April 2020; accepted 5 May 2020; published 1 June 2020)

The spin-$\frac{1}{2}$ Heisenberg antiferromagnetic chain is ideal for realizing one of the simplest gapless quantum spin liquids (QSLs), supporting a many-body ground state whose elementary excitations are fractional fermionic excitations called spinons. Here we report the discovery of such a one-dimensional (1D) QSL in $Cs_4CuSb_2Cl_{12}$. Compared to previously reported $S = \frac{1}{2}$ 1D chains, this material possesses a wider temperature range over which the QSL state is stabilized. We identify spinon excitations extending at $T > 0.8$ K, with a large T-linear contribution to the specific heat, $\gamma = 31.5(2)$ mJ mol^{-1} K^{-2}, which contribute itinerantly to thermal transport up to temperatures as high as $T = 35$ K. At $T = 0.7$ K, we find a second-order phase transition that is unchanged by a $\mu_0 H = 5$ T magnetic field. $Cs_4CuSb_2Cl_{12}$ reveals new phenomenology deep in the 1D QSL regime, supporting a gapped QSL phase over a wide temperature range compared to many other experimental realizations.

DOI: 10.1103/PhysRevB.101.235107

I. INTRODUCTION

Quasi-1D magnets exhibit an incredibly rich variety of physics, and there is much phenomenology completely unique to one-dimensional (1D) spin-systems. In 2D and 3D magnets, competing exchange interactions are requisite for the frustration and strong quantum fluctuations that drive novel states of matter such as quantum spin liquids (QSLs) [1–4]. As such, there are a variety of QSLs hypothesized to exist within different lattice symmetries (2D: triangular, kagome, honeycomb; 3D: pyrochlore, diamond, hyperkagome) and various types of magnetic exchange (Heisenberg, Kitaev, Dzyaloshinskii-Moriya) [2–14]. In contrast to these higher-dimensional examples, quasi-1D quantum magnets are an excellent platform for realizing QSLs without frustration. In particular, the quantum 1D $S = \frac{1}{2}$ Heisenberg antiferromagnetic chain (HAFC) is an important theoretical paradigm with emergent collective behavior that realizes a gapless QSL. The idealized model, which considers only nearest-neighbor interactions:

$$H = J \sum_{\langle ij \rangle} \boldsymbol{S}_i \cdot \boldsymbol{S}_j, \tag{1}$$

has an exactly solvable ground state that is a macroscopically entangled QSL state given by the Bethe ansatz [15–24]. In this many-body state, the elementary excitation of the HAFC is a type of fractional fermionic quasiparticle called a spinon, which carries spin-$\frac{1}{2}$. Thermodynamically, spinons may be identified in an insulating magnet by a distinct T-linear contribution to the specific heat at temperatures $T \ll J/k_B$ and their field-dependent itinerant contribution to thermal conductivity [25].

One of the first experimental realizations of the $S = \frac{1}{2}$ HAFC was discovered in $CuGeO_3$ [18]. This material undergoes a magnetic phase transition to a long-range ordered spin-Peierls state at $T = 14$ K [18,26]. Another seminal example of an $S = \frac{1}{2}$ HAFC is Sr_2CuO_3 [27–29]. This system exhibits very strong intrachain exchange coupling J/k_B yet also undergoes a 3D magnetic phase transition at $T \approx 5$ K [27]. Indeed, in most real quasi-1D systems the viable temperature range over which QSL physics or spinonlike excitations may be observed is limited by the fact that interchain couplings will eventually stabilize 3D long-range order, or by the fact that dimerization at low enough temperatures will favor a state of localized spin-singlets supporting gapped bosonic excitations.

In this paper, we report the discovery of a QSL $S = \frac{1}{2}$ HAFC in the material $Cs_4CuSb_2Cl_{12}$ (CCSC). It features a wide temperature window over which the QSL state is stabilized. We observe spinon excitations at $T > 0.8$ K, characterized by a large T-linear contribution $\gamma = 31.5(2)$ mJ mol^{-1} K^{-2} to the specific heat that extends to at least 5 K, deducing an intrachain exchange coupling $J/k_B = 176(2)$ K. We additionally report evidence of a second-order phase transition at $T_c = 0.7$ K, finding an anomaly in the

*mcqueen@jhu.edu

specific heat that is insensitive to applied fields up to $\mu_0 H = 5$ T, suggesting the existence of a weak second-order phase transition. This transition is reminiscent of a spin-Peierls transition into a low-T partially spin-dimerized state, however this time we find only limited evidence in favor of a spin-gap opening at $T < T_c$, thus further investigation is required to deduce the nature of the low-T phase. Further investigation of thermal transport reveals a field dependence up to as high as $T = 35$ K associated with an itinerant magnetic contribution, suggesting that spinonlike excitations in CCSC persist up to temperatures as high as $0.2J/k_B$.

II. EXPERIMENT

Polycrystalline CCSC was synthesized through solid-state reactions at 220 °C for 3 days by combining stoichiometric amounts of CsCl, $CuCl_2$, and $SbCl_3$. Dark purple triangular-shaped crystals of CCSC were grown by hydrothermal techniques. The reaction mixture of 1 g of polycrystalline CCSC and 10 mL of 12 M HCl was placed in a 23-mL Teflon-lined stainless-steel autoclave. The autoclave was closed, gradually heated up to 150 °C, held for 3 days, and then slowly cooled to room temperature at a rate of 6 °C h^{-1}.

Powder x-ray diffraction (PXRD) data were collected at room temperature using a Bruker D8 Focus diffractometer with a LynxEye detector using Cu $K\alpha$ radiation ($\lambda = 1.5424$ Å). Rietveld refinements on PXRD data were performed using TOPAS 4.2.

Single-crystal x-ray diffraction (SXRD) data were collected at $T = 213$ K using the program CRYSALISPRO (Version 1.171.36.32 Agilent Technologies, 2013) on a SuperNova diffractometer equipped with an Atlas detector using graphite-monochromated Mo $K\alpha$ ($\lambda = 0.710\,73$ Å). CRYSALISPRO was used to refine the unit-cell dimensions and for data reduction. The temperature of the sample was controlled using the internal Oxford Instrument Cryojet. The structure was solved using SHELXL-97 and refined using SHELXL-97. All calculations were performed using the SHELXL-97 crystallographic software package [30].

Powder neutron diffraction data were collected using the time-of-flight high-flux NOMAD at the Spallation Neutron Source, Oak Ridge National Laboratory. Rietveld refinements were performed using GSAS in EXPGUI [31].

Physical property characterization was performed using the Quantum Design Physical Properties Measurement System (PPMS). Magnetization data were collected using the VSM options at $T = 2-300$ K under $\mu_0 H = 5$ T and converted to magnetic susceptibility using the approximation $\chi = M/H$. Heat-capacity data were collected using the semiadiabatic pulse technique (2% heat rise) for $T = 0.2-300$ K.

Density functional calculations are carried out by using the projector augmented-wave method implemented in the Vienna ab initio simulation package (VASP) [32,33]. The recently developed strongly constrained and appropriately normed (SCAN) density functional is used to treat the exchange-correlation interactions [34]. The SCAN functional is able to stabilize the magnetic moment on Cu, while the conventional local density approximation (LDA) and generalized gradient approximation (GGA) fail to do so. An energy cutoff of 500 eV is to truncate the plane-wave basis, and a $4 \times 4 \times 4$ K mesh is used in sampling the Brillouin zone of a 76-atom cell. All calculations are done with the experimental crystal structure.

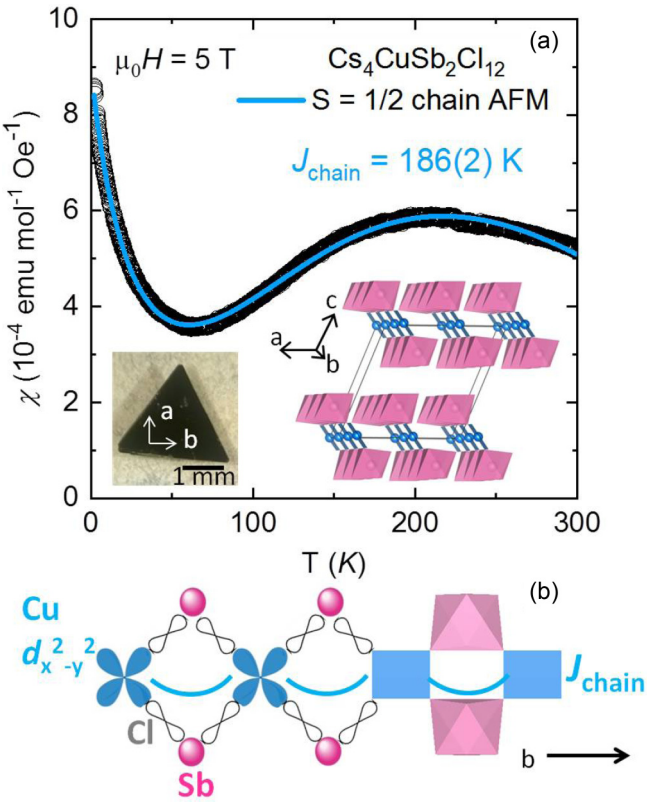

FIG. 1. (a) The magnetic susceptibility of $Cs_4CuSb_2Cl_{12}$ as a function of temperature. An $S = \frac{1}{2}$ HAFC model gives an intrachain exchange coupling of $J/k_B = 186(2)$ K. Inset: single crystal and overall crystal structure. (b) The structure of the 1D chains of $Cs_4CuSb_2Cl_{12}$, showing the superexchange interactions along the b-axis.

The in-plane longitudinal thermal conductivity $\kappa_{xx} \equiv \kappa$ was measured on an as-grown sample of dimension approximately $1 \times 0.5 \times 0.2$ mm^3, using a single-heater, two-thermometer configuration in steady-state operation with magnetic field applied either in the ab plane ($H||\nabla T||ab$) or normal to the plane ($H||c$). Over the entire temperature range of measurement, the difference in absolute temperatures across the sample was set so that it never exceeded 5% of the bath temperature. All thermometry was performed using CERNOX chip resistors, which were precalibrated individually and *in situ*, both with and without applied fields.

III. MAGNETISM

The structure of CCSC consists of $S = \frac{1}{2}$ $CuCl_4$ plaquettes connected by Sb ions to form 1D chains, Fig. 1. The magnetic susceptibility, measured at $\mu_0 H = 5$ T and estimated as $\chi \approx M/H$, shows a broad maximum around $T = 210$ K, followed by an upturn below $T = 50$ K. This behavior is characteristic of an $S = \frac{1}{2}$ HAFC in the presence of a few magnetic impurity spins [15,18,21,27,35]. No indication of a transition to a 3D long-range-ordered magnetic state is observed in magnetization measurements at temperatures $T > 2$ K.

TABLE I. Crystallographic data for $Cs_4CuSb_2Cl_{12}$, S.G.$C2/m$ (No. 12), $a = 13.083(3)$ Å, $b = 7.3507(2)$ Å, $c = 13.070(3)$ Å, and $\beta = 112.17(3)^\circ$.

	x	y	z	s.o.f.	U_{iso}
Cs1	0.1241(2)	0.0000	0.3698(2)	1	0.0229(9)
Cs2	0.3745(2)	0.0000	0.1199(2)	1	0.0243(9)
Sb1	0.2520(2)	0.5000	0.2586(2)	1	0.0127(9)
Cu1	0.0000	0.0000	0.0000	1	0.0142(2)
Cl1	0.1119(5)	0.2206(8)	0.1106(5)	1	0.0243(2)
Cl2	0.3739(6)	0.5000	0.1353(6)	1	0.0238(2)
Cl3	0.3693(4)	0.2626(7)	0.3728(4)	1	0.0239(2)
Cl4	0.1345(6)	0.5000	0.3769(6)	1	0.0239(2)

Quantitative analysis was performed by using the $S = \frac{1}{2}$ HAFC Bonner-Fisher model plus a Curie-Weiss term for the defect spins [17,36–38],

$$\chi = \chi_{BF}(J, T) + C/(T - \theta), \tag{2}$$

where χ is the observed susceptibility, J is the intrachain exchange interaction, and C and θ are the Curie constant and Weiss temperature for the defect spins. An optimized fit to the data gives $J/k_B = 186(2)$ K, $C = 0.011(1)$ emu mol f.u.$^{-1}$ Oe^{-1} K, and $\theta = -9.2(3)$ K. The chain interaction strength is consistent with the location of the observed maxima of χ and additionally consistent with an alternative fit utilizing a dimer model (not shown). The Curie constant corresponds to ~3% of $S = \frac{1}{2}$ impurity spins, and the corresponding Weiss temperature indicates a reasonable interaction strength as would be expected for isolated $S = \frac{1}{2}$ units in unsaturated coordination environments between the units and the chains.

The broad maximum feature of the magnetic susceptibility of $Cs_4CuSb_2Cl_{12}$ at $T \sim 210$ K [Fig. 1(a)] could indicate that the spins were already paired up at high temperature $T > 300$ K. To unambiguously rule out this possibility, time-of-flight neutron powder diffraction (TOF-NPD) measurements were performed at $T = 300$ K by NOMAD. The TOF-NPD patterns were simultaneously analyzed by Rietveld refinements in order to determine the presence or absence of magnetic ordering. The data were fit well with the crystal structure of $Cs_4CuSb_2Cl_{12}$ and no additional Bragg peaks attributed to magnetic ordering of any kind are observed. As a test, a magnetic phase was added to the refinement to assess whether magnetic scattering would be visible. To estimate the sensitivity to magnetic order, we used an AFM state. This yielded an upper limit on the magnetic moment of $0.2(5)\,\mu_B$ per Cu.

To further explore the exchange coupling in this system and verify its quasi-1D nature as an $S = \frac{1}{2}$ HAFC, we performed density functional theory calculations using the recently developed strongly constrained and appropriately normed (SCAN) exchange correlation functional [39]. We used CCSC crystal structure determined from TOF-NPD and x-ray diffraction measurements, Table I [40].

Results of our calculations are shown in Fig. 2. The magnetic density on Cu sites clearly reveals that $d_{x^2-y^2}$ orbitals are polarized, direct evidence of $3d$ [9] Cu^{2+} cations with

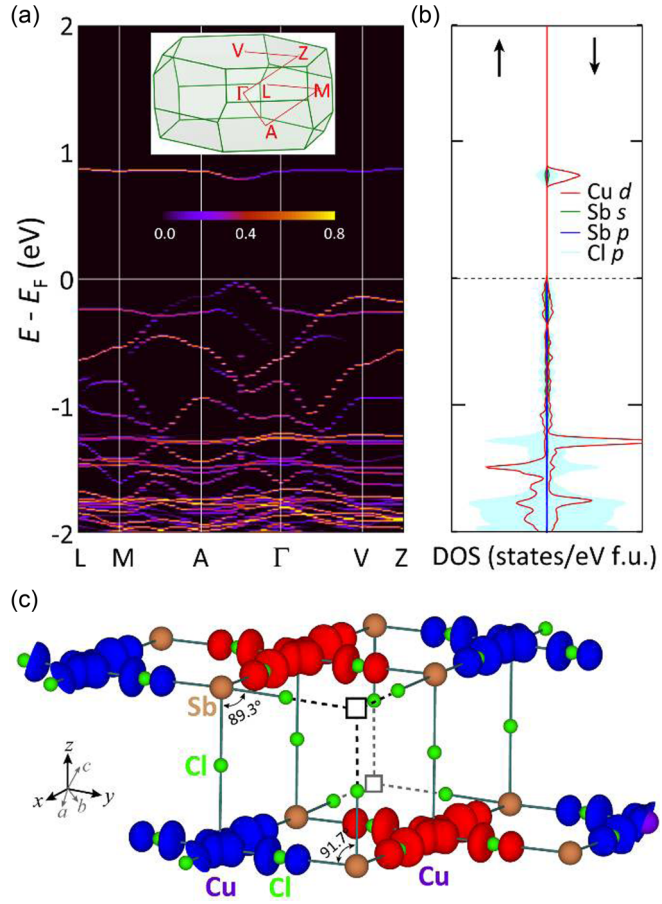

FIG. 2. (a) Unfolded band structure of the $Cs_4CuSb_2Cl_{12}$ AFM 1D chain. The unfolding maps the band structure of the $2\times2\times1$ AFM supercell into that of the $1\times1\times1$ nonmagnetic primitive cell, and a weaker spectral weight (purple color on the left end of the color bar) indicates that the band structure is more significantly affected by the magnetism. The inset shows the band path in the primitive cell Brillouin zone. (b) Spin-polarized density of states (DOS). (c) Calculated magnetic density. The red and blue isosurfaces denote the spin-up and spin-down charge densities, respectively. Cu ions form AFM chains within the xy-plane, but they do not have magnetic coupling across the planes. The open squares (□) denote empty sites.

effective $S = \frac{1}{2}$. Within the ab plane, the spin of Cu^{2+} also polarizes the p_x and p_y electrons on the four Cl ligand anions, forming $CuCl_4$ units with AF couplings along the b-axis. We have observed similar spin polarization of oxygen in cuprates [34,41]. To estimate the strength of the exchange coupling J, the total energies of the antiferromagnetic (AFM) and ferromagnetic (FM) states of the nearest-neighbor $S = \frac{1}{2}$ Heisenberg Hamiltonian in the mean-field approximation were calculated. The difference in total energies of the AFM and FM phases is given by

$$\Delta E = E_{AFM} - E_{FM} = JNZ\langle S\rangle^2, \tag{3}$$

where N is the total number of magnetic moments, Z is the number of nearest-neighbor spins, and $\langle S\rangle$ is the averaged spin on each site. Because the spin density supports the predominance of intrachain interactions, we take $Z = 2$. These calculations were normalized to one formula unit, so $N = 1$.

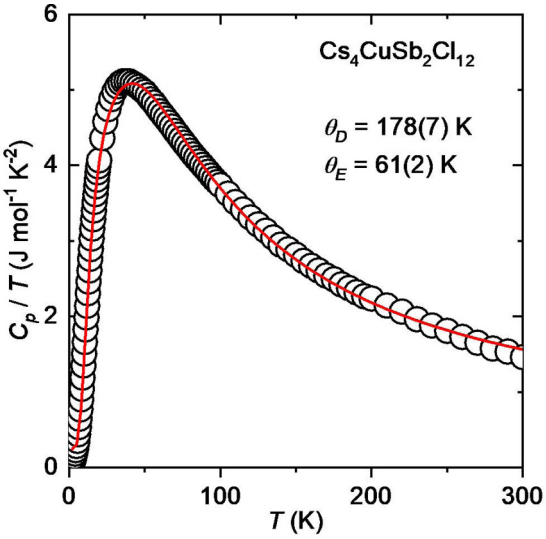

FIG. 3. The specific heat C_p/T vs T of CCSC from $T = 2$ to 300 K shows no sharp anomalies, indicative of a lack of long-range magnetic ordering or other phase transitions. The circles and the solid line correspond to the data and fit to Eq. (5), respectively.

Our first-principles computations for the total energies of the AFM and FM states resulted in a predicted $J/k_B \sim 200$ K (depending on the precise approximations used), lending further plausibility to the experimentally determined J/k_B value of 186(2) K deduced from susceptibility fits, and our analysis of the specific heat.

We calculate a Cu magnetic moment of 0.52 μ_B. Note that there is also considerable contribution to the magnetization from Cl ligands, with each Cl contributing an additional magnetic moment of 0.06 μ_B. The theoretical band gap calculated is 0.28 eV, smaller than the experimental value of ~1 eV estimated from UV-vis spectroscopy measurements. The valence-band maximum is mostly composed of the Cu-$d_{x^2-y^2}$, Cl-p, and Sb-s states. The conduction-band minimum is isolated from other bands, and mainly derived from Cu $d_{x^2-y^2}$ states with some hybridized Cl-p states. Thus, DFT calculations also support CCSC as a realization of a 1D HAFC.

IV. HEAT CAPACITY

To elucidate the thermodynamics of the ground state, we performed heat-capacity measurements over the range $0.2 \leqslant T \leqslant 300$ K. For $T \geqslant 2$ K, there are no sharp anomalies, indicative of a lack of long-range magnetic ordering or other phase transitions (Fig. 3). The heat-capacity data above $T = 2$ K are modeled very well with one Einstein mode $[E(\theta_E, T)]$, one Debye mode $[D(\theta_D, T)]$, and magnetic contribution (γ) following the equation

$$C_p/T = E(\theta_E, T)/T + D(\theta_D, T)/T + \gamma. \quad (4)$$

The Einstein and Debye temperature can be extracted from the fit to be 61(2) and 178(7) K, respectively.

There is, however, an apparent T-linear contribution that extends up to at least $T = 5$ K. To further explore this contribution, expected for a 1D HAFC QSL [17,42], we performed specific-heat measurements in a Quantum Design PPMS dilution refrigerator from $T = 0.2$ to 3 K, Fig. 4.

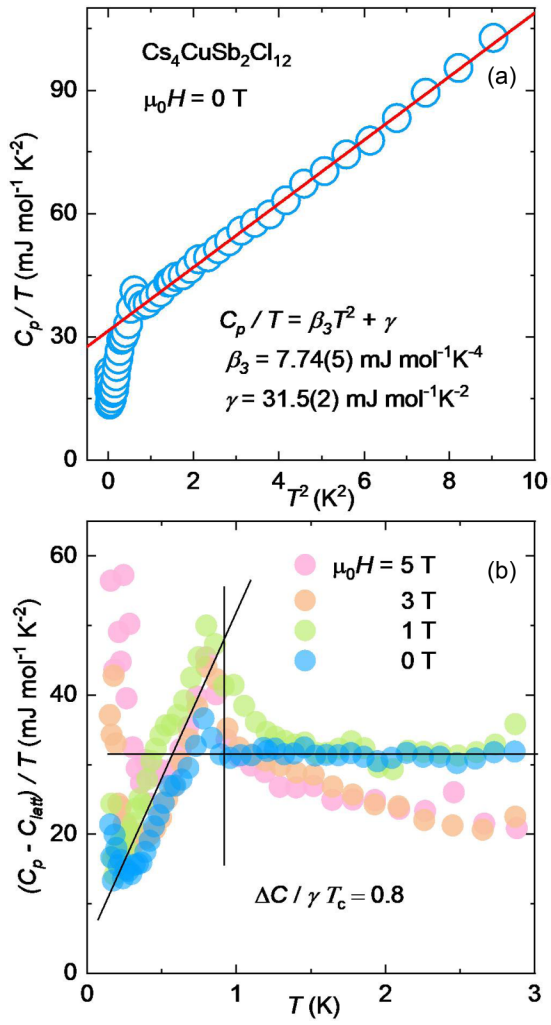

FIG. 4. (a) Low-temperature heat capacity of the CCSC C_p/T vs T^2 plot shows the existence of a linear correlation from which phononic and magnetic contributions can be extracted; (b) $(C_p - C_{latt})/T$ vs T plot depicts the second-order phase transition.

T-power-law behavior of the heat capacity at low temperatures is deeply informative about the nature of low-energy quasiparticle excitations. The power-law exponent is not only telling of the dimensionality of the excitations, which modifies the density of states, but also indicative of their dispersion $\varepsilon(k)$ at zone center, as for bosonic and fermionic statistics alike, contributions from all other parts of the excitation spectrum are exponentially suppressed as $\exp(-\varepsilon/k_B T)$ at low T. In virtually every insulator, the most obvious low-T contribution to the heat capacity is a T^3 phononic term, describable via the Debye model. In a magnetic insulator, the presence of a large T-linear contribution is strongly indicative of low-dimensional magnetic excitations, and only a few combinations of dimensionality and low-k dispersion can theoretically produce precisely $C \sim T$. In the context of CCSC, 1D spinons are the only plausible source of such a sizable linear contribution. The predicted T-linear spinon contribution intrinsic to the HAFC QSL is given by [43,45]

$$\gamma = \tfrac{2}{3} R k_B / J, \quad (5)$$

where J is the AFM intrachain exchange interaction strength. Between $0.7 < T < 3$ K, we find that the total specific heat is well-modeled by the following equation, as shown in Fig. 4(a):

$$C_p/T = \gamma + \beta_3 T^2, \tag{6}$$

including terms for the expected magnetic ($C_{\rm m} = \gamma T$) and phononic ($C_{\rm latt} = \beta_3 T^3$ [3]) contributions to the specific heat. An optimized fit yields values of $\gamma = 31.5(2)\,{\rm mJ\,mol^{-1}\,K^{-2}}$ and $\beta_3 = 7.74(5)\,{\rm mJ\,mol^{-1}\,K^{-4}}$, respectively. From the above formula for γ, we deduce an exchange coupling $J/k_{\rm B} = 176(2)$ K, which is in excellent agreement with the $J/k_{\rm B} = 186(2)$ K determined from the magnetic susceptibility.

This T-linear term is disrupted by a phase transition at $T_c = 0.7$ K. The λ-like anomaly is characteristic of a second-order phase transition. The concomitant loss of the majority of the T-linear contribution suggests that spinon excitations are partially or entirely gapped, which might occur in the scenario that spins of the 1D chain dimerize at $T < T_{\rm C}$, undergoing spin-Peierls transition. It has been observed in other 1D HAFC systems [18,29] and it is also plausible in CCSC. Further investigation, via neutron scattering in particular, could clarify the nature of the transition we have observed.

Application of a $\mu_0 H = 5$ T magnetic field does not suppress or move the transition within the resolution of our measurements, suggesting that the phase transition is weakly coupled to the applied field. Taken together, these results imply the γ term is intrinsic to CCSC, not due to disorder or impurity spins, and necessarily a consequence of fermionic spinon excitations, i.e., gapless excitations in the QSL state [16,23,44,45].

The upturns of specific heat at $T < 250$ mK can be attributed to nuclear Schottky contribution of Sb. The temperature for the manifestation is consistent with that for Sb [46]. In addition, the nuclear Schottky contribution of Sb is likely more pronounced than that of Cu for the following two reasons: (i) the spins of two abundant isotopes of Sb are 5/2 and 7/2 for ^{121}Sb and ^{123}Sb, respectively, while that of both ^{63}Cu and ^{65}Cu is 3/2; and (ii) the amount of Sb is two times more than that of Cu per formula unit.

V. THERMAL CONDUCTIVITY

Now we turn to the Thermal Conductivity in CCSC. Figure 5 shows κ as a function of temperature for zero field (ZF) and the maximum field applied, $\mu_0 H = 18$ T. We checked the field dependence of κ in both in-plane and out-of-plane orientations and found it is completely insensitive to the direction of the applied field. For ZF and 18 T, conspicuous peaks of similar size occur at the same temperature, approximately 8 K, followed by a rapid decrease of κ, as T is further lowered even below $T_c = 0.7$ K. At the peak, the suppression in κ is about 10% of the ZF value and it is observed only in $3 \lesssim T \lesssim 35$ K. At low temperatures, $T < 3$ K, κ becomes field-independent up to 18 T and follows a power-law dependence with approximate exponent $\kappa \sim T^{1.8}$ (see the inset of Fig. 5). Our measurement bears many similarities to thermal conductivity data measured in the $S = \frac{1}{2}$ 1D HAFC chain cuprate Sr_2CuO_3 [28], namely (i) thermal conductivity in the low-T ballistic regime also follows a subquadratic T-dependence, and (ii) despite a significant T-linear contribution to the heat capacity in the disordered QSL phase, an itinerant spinon contribution is not obvious. Even in the low-T ballistic limit, the total thermal conductivity $\kappa_{\rm tot} = \kappa_{\rm ph} + \kappa_{\rm sp}$, corresponding to a sum of phonon ($\kappa_{\rm ph}$) and spinon ($\kappa_{\rm sp}$) contributions, cannot be described simply as a sum of independent T^3 phonon and T-linear spinon contributions proportional to $C_{\rm latt}$ and $C_{\rm m}$, respectively. The observed T dependence, which is power-law-like and subquadratic in T, is not adequately captured with the combination of two such terms alone.

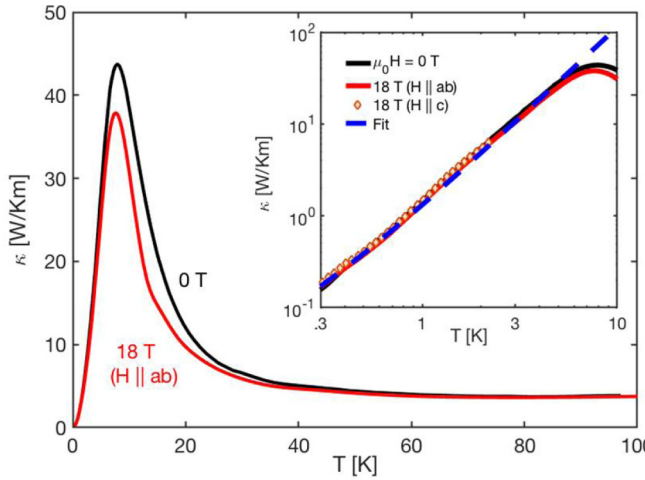

FIG. 5. κ shown as a function T for 0 T (ZF) and 18 T applied normal to the plane. Temperature gradient was in the *ab* plane. Inset $\kappa(T)$ shown on a logarithmic scale for comparison of the low-T data at different fields. The dotted blue line illustrates a fit using Eq. (10) where $\tau_{\text{sp-ph}}$ is assumed to be T-linear. See the text for details.

In the framework of the Debye-Callaway model [61,62], phonon thermal conductivity is expressed as

$$\kappa_{\rm ph} = \frac{k_{\rm B}}{2\pi^2 v_{\rm ph}} \int_0^{\theta_{\rm D}/T} \frac{x^4 e^x}{(e^x - 1)^2} \tau_{\rm ph}(x) dx, \tag{7}$$

where $v_{\rm ph}$ and $\tau_{\rm ph}$ are the speed of sound and phonon relaxation time, respectively, and $x = \hbar\omega_{\rm ph}/k_{\rm B}T$, where $\omega_{\rm ph}$ is the acoustic phonon frequency. In the nearly ballistic limit, which our analysis focuses on, $\tau_{\rm ph}$ can be treated as mode-independent [$\tau_{\rm ph}(x) = \tau_{\rm ph} = {\rm const}$], yielding the simplification $\kappa_{\rm ph} = \frac{1}{3} C_{\rm latt} {v_{\rm ph}}^2 \tau_{\rm ph}$ in terms of the Debye phonon heat capacity $C_{\rm latt}$ as shown in Fig. 4(a). In the ballistic limit, the phonon mean free path $l_{\rm ph,0}$, arising from phonon-phonon scattering is limited by the boundary scattering, and thus $l_{\rm ph,0}$ should be on the order of the sample dimension and T-independent.

To account for spin-induced scattering of phonons, we include the spin-phonon relaxation time $\tau_{\text{sp-ph}}$ via Matthiessen's rule. By exact analogy to Eq. (7) for the spinon contribution, we arrive at the following expression for the total thermal conductivity in a nearly ballistic limit with allowed spin-phonon interaction:

$$\kappa_{\rm tot} = \tfrac{1}{3} C_{\rm latt} v_{\rm ph} \left[l_{\rm ph,0}^{-1} + (v_{\rm ph} \tau_{\text{sp-ph}})^{-1} \right]^{-1} + C_{\rm m} v_{\rm sp} \left[l_{\rm sp,0}^{-1} + (v_{\rm sp} \tau_{\text{sp-ph}})^{-1} \right]^{-1}, \tag{8}$$

where v_{sp} and $l_{sp,0}$ correspond, respectively, to the average spinon propagation speed and intrinsic spinon mean free path, i.e., in the absence of scattering with phonons. v_{ph} and v_{sp} are calculated from the parameters β_3 and γ, respectively, assuming Debye-like phonons and spinons following a Cloizeaux-Pearson dispersion [63]. The lack of strong T-linear or sublinear behavior in our κ data implies that thermally excited spinons are only coherent over small length scales ($l_{sp,0} \ll l_{ph,0}$), and their contribution to thermal transport is minimal. To account for the unusual T-dependence in this ballistic regime, $\kappa \sim T^{1.8}$, we assume that ${\tau_{sp\text{-}ph}}^{-1}$ is directly proportional to the density of magnetic excitations, which our analysis of the heat capacity has found to be T-linear. We fit data in the range $0.3 < T < 3$ K to Eq. (8) with three free parameters: $l_{ph,0}$, $l_{sp,0}$, and $\tau_{sp\text{-}ph}$, the results of which are shown in the inset of Fig. 5. The best fit is obtained with $l_{ph,0} = 880(50)\,\mu$m, $l_{sp,0} = 270(40)$ nm, and $\tau_{sp\text{-}ph}(1\,\text{K}) = 65(2)$ ns.

The resulting fit-parameter values are found to be consistent with the presumed regime of $l_{sp,0} \ll v_{ph}\tau_{sp\text{-}ph} \ll l_{ph,0}$. $l_{ph,0}$ is approximately $\simeq$1 mm (the length of the sample in the direction of ∇T) while the spin-phonon relaxation time at $T = 1$ K corresponds to a phonon scattering length by spinons (i.e., $v_{ph}\tau_{sp\text{-}ph}$) of $\simeq$100 μm, about 10% of $l_{ph,0}$. Our fit suggests that $l_{sp,0}$ is less than $l_{ph,0}$, by a factor of 10^3. Such a short intrinsic spinon scattering length scale, possibly due to impurity spin scattering, accounts for the negligible contribution of coherent spinons to heat transport below 3 K. The hierarchy of phonon scattering length scales suggests that the time/length scale for spin-phonon interaction is much smaller than that for boundary-limited collisions, hence spin-phonon interaction sets the dominant scale for phonon scattering. Consequently, the temperature dependence of $\tau_{sp\text{-}ph}(T)$ is likely the main factor responsible for the deviations of $\kappa(T)$ from the T^3 behavior of C_{latt} in this regime.

At intermediate temperatures, $3 < T < 35$ K, it is plausible that 1D HAFC spinons with a gapless linear dispersion contribute to coherent heat transport. While the intrinsic scattering spinon length scale at low T is quite small relative to that for phonons, the situation may quickly change with increasing temperature. Away from a ballistic regime, umklapp phonon-phonon scattering processes typically reduce the minimum phonon scattering length by several orders of magnitude. As applied field increases, the suppression of the total κ near the peak may be attributed to the coexistence of both types of heat carrier—phonons and spinons—over similar length scales. An applied field can gap spin excitations, leading to the reduction of spinon populations and overall κ. The magnetic contribution finally becomes insignificant at $T > 35$ K, where the field dependence disappears once again. This finding suggests that spinonlike excitations must persist up to at least $T \simeq 0.2\,J/k_B$.

VI. CONCLUSIONS

CCSC harbors a nearly ideal HAFC QSL state, with a weak spin-Peierls transition at $T = 0.7$ K. CCSC has a large temperature window over which the QSL state is stable, as judged by the ratio of the intrachain interaction strength to the ordering or phase transition temperature, Table II. $KCuGaF_6$ was also realized as a $S = \frac{1}{2}$ HAFC with $J/k_B = 100$ K [43].

TABLE II. A summary of the exchange interaction J/k_B, transition temperature T_c, and normalized factor $(J/k_B)/T_c$ of $Cs_4CuSb_2Cl_{12}$ and the other $S = \frac{1}{2}$ HAFCs.

Compound	J/k_B(K)	T_c(K)	$(J/k_B)/T_c$	Ref.
Sr_2CuO_3	2200	5	440	[27,48]
$Sr_2Cu(PO_4)_2$	144	0.45	320	[49]
$Ba_2Cu(PO_4)_2$	132	0.45	293	[49]
$Cs_4CuSb_2Cl_{12}$	186	0.7	270	This work
$KCuMoO_4(OH)$	238	1.5	160	[21]
$BaCuP_2O_7$	104	0.8	130	[50]
Nd_2CuO_4	156	1.5	104	[35]
$BaCu_2Ge_2O_7$	540	8.8	61	[51]
$Bi_6V_3O_{16}$	113	2	60	[47]
Sm_2CuO_4	189	5.9	32	[35]
$BaCu_2Si_2O_7$	280	9.2	30	[20]
$VOSb_2O_4$	245	14	18	[52]
$TiPO_4$	965	74	13	[53]
TiOBr	375	28	13	[54]
TiOCl	660	67	10	[55]
$KCuF_3$	395	39	10	[56]
$CuGeO_3$	88	14	6.3	[18]
$CuSb_2O_6$	48	9	6	[57]
$CuCl_2$	90	24	3.8	[58]
$CuSiO_3$	21	8	2.6	[59]
Cs_2CuCl_4	2	1	2	[60]

However, the nuclear Schottky contribution becomes overwhelming at low temperature, hindering study of the physics deep in the QSL phase [43]. $LiCuSbO_4$ features a complex frustrated 1D chain, which cannot be solely described by the HAFC model [15]. $Bi_6V_3O_{16}$ was reported to exhibit an $S = \frac{1}{2}$ uniform HAFC with $J/k_B = 100$ K, nevertheless further knowledge of a possible ordering temperature deep in the 1D QSL regime is needed [47]. Of many extensively studied $S = \frac{1}{2}$ HAFC systems, CCSC exhibits a large factor of $(J/k_B)/T_c$, indicative of the wide temperature window over which the QSL is stabilized. This is further supported by the apparent effect of spinons on thermal transport, contributing itinerantly at temperatures as high as $T = 35$ K, and potentially setting the shortest timescale for low-T phonon scattering.

In summary, we have provided evidence of spinon QSL physics in the insulating material CCSC. This realization of a QSL in this $S = \frac{1}{2}$ HAFC was deduced from the results of magnetic susceptibility, specific heat, neutron diffraction, thermal transport, and DFT computations. CCSC differs from other quantum HAFC systems for the following reasons: (i) the temperature window over which a QSL is stabilized is large compared to other examples, (ii) spinon excitations extending from $T > 0.8$ K with a large $\gamma = 31.5(2)$ mJ mol^{-1} K^{-2} contribution are identified and they continue to play a role in thermal transport up to $T \sim$35 K, and (iii) a second-order weak phase transition is observed that is insensitive to applied fields up to $\mu_0 H = 5$ T, suggesting a robust spin-stiffness in the vicinity of the phase transition. Additional characterizations including ultrasound and inelastic neutron scattering are underway to help gain a better understanding of the underlying physics and its unique

ability to stabilize QSL over such a wide temperature range in this system.

ACKNOWLEDGMENTS

This work was supported as part of the Institute for Quantum Matter, an Energy Frontier Research Center funded by the U.S. Department of Energy, Office of Science, Office of Basic Energy Sciences, under Award No. DE-SC0019331. We acknowledge the support from Johns Hopkins University, Krieger School of Art and Sciences, Faculty Innovation Award, and the Johns Hopkins University Discovery Award. The dilution refrigerator was funded by the National Science Foundation, Division of Materials Research, Award No. 0821005. The research at Oak Ridge National Laboratory's Spallation Neutron Source was sponsored by the U.S. Department of Energy, Office of Basic Energy Sciences, Scientific User Facilities Division. J.S. and Y.Z. were supported by the U.S. Department of Energy under EPSCoR Grant No. DE-SC0012432 with additional support from the Louisiana Board of Regents. M.J.W. was supported by the Foundation for Polish Science (FNP). T.T.T. acknowledges the support from Clemson University (start-up funding). C.A.P. acknowledges the support of the Colorado Energy Research Collaboratory. A portion of this work was performed at the National High Magnetic Field Laboratory, which is supported by National Science Foundation Cooperative Agreement No. DMR-1644779 and by the State of Florida.

[1] S. Sachdev, Science **288**, 475 (2000).
[2] L. Balents, Nature (London) **464**, 199 (2010).
[3] Y. Zhou, K. Kanoda, and T.-K. Ng, Rev. Mod. Phys. **89**, 025003 (2017).
[4] L. Savary and L. Balents, Rep. Prog. Phys. **80**, 016502 (2017).
[5] P. A. Lee, Science **321**, 1306 (2008).
[6] P. W. Anderson, Mater. Res. Bull. **8**, 153 (1973).
[7] Y. Shimizu, K. Miyagawa, K. Kanoda, M. Maesato, and G. Saito, Phys. Rev. Lett. **91**, 107001 (2003).
[8] J. A. M. Paddison, M. Daum, Z. Dun, G. Ehlers, Y. Liu, M. B. Stone, H. Zhou, and M. Mourigal, Nat. Phys. **13**, 117 (2017).
[9] J. J. Wen, S. M. Koohpayeh, K. A. Ross, B. A. Trump, T. M. McQueen, K. Kimura, S. Nakatsuji, Y. Qiu, D. M. Pajerowski, J. R. D. Copley, and C. L. Broholm, Phys. Rev. Lett. **118**, 107206 (2017).
[10] X. Bai, J. A. M. Paddison, E. Kapit, S. M. Koohpayeh, J. J. Wen, S. E. Dutton, A. T. Savici, A. I. Kolesnikov, G. E. Granroth, C. L. Broholm, J. T. Chalker, and M. Mourigal, Phys. Rev. Lett. **122**, 097201 (2019).
[11] S. Zhang, H. J. Changlani, K. W. Plumb, O. Tchernyshyov, and R. Moessner, Phys. Rev. Lett. **122**, 167203 (2019).
[12] Y. Li, S. M. Winter, and R. Valentí, Phys. Rev. Lett. **121**, 247202 (2018).
[13] P. Mendels and F. Bert, C. R. Phys. **17**, 455 (2016).
[14] Q. Liu, Q. Yao, Z. A. Kelly, C. M. Pasco, T. M. McQueen, S. Lany, and A. Zunger, Phys. Rev. Lett. **121**, 186402 (2018).
[15] S. E. Dutton, M. Kumar, M. Mourigal, Z. G. Soos, J. J. Wen, C. L. Broholm, N. H. Andersen, Q. Huang, M. Zbiri, R. Toft-Petersen, and R. J. Cava, Phys. Rev. Lett. **108**, 187206 (2012).
[16] B. Lake, D. A. Tennant, J. S. Caux, T. Barthel, U. Schollwock, S. E. Nagler, and C. D. Frost, Phys. Rev. Lett. **111**, 137205 (2013).
[17] D. C. Johnston, R. K. Kremer, M. Troyer, X. Wang, A. Klumper, S. L. Bud'ko, A. F. Panchula, and P. C. Canfield, Phys. Rev. B **61**, 9558 (2000).
[18] M. Hase, I. Terasaki, and K. Uchinokura, Phys. Rev. Lett. **70**, 3651 (1993).
[19] J. W. Bray, H. R. Hart, Jr., L. V. Interrante, I. S. Jacobs, J. S. Kasper, G. D. Watkins, S. H. Wee, and J. C. Bonner, in *Magnetism and Magnetic Materials-1975*, edited by J. J. Becker, G. H. Lander and J. J. Rhyne, AIP Conf. Proc. No. 29 (AIP, New York, 1976), p. 504.
[20] I. Tsukada, Y. Sasago, K. Uchinokura, A. Zheludev, S. Maslov, G. Shirane, K. Kakurai, and E. Ressouche, Phys. Rev. B **60**, 6601 (1999).
[21] K. Nawa, O. Janson, and Z. Hiroi, Phys. Rev. B **96**, 104429 (2017).
[22] I. Affleck and M. Oshikawa, Phys. Rev. B **60**, 1038 (1999).
[23] S. Yamashita, Y. Nakazawa, M. Oguni, Y. Oshima, H. Nojiri, Y. Shimizu, K. Miyagawa, and K. Kanoda, Nat. Phys. **4**, 459 (2008).
[24] S. Fujiyama and R. Kato, Phys. Rev. Lett. **122**, 147204 (2019).
[25] W. McRae and O. P. Sushkov, Phys. Rev. B **58**, 62 (1998).
[26] M. Weiden, J. Koehler, G. Sparn, M. Koeppen, M. Lang, C. Geibel, and F. Steglich, Z. Phys. B **98**, 167 (1995).
[27] N. Motoyama, H. Eisaki, and S. Uchida, Phys. Rev. Lett. **76**, 3212 (1996).
[28] A. V. Sologubenko, E. Felder, K. Gianno, H. R. Ott, A. Vietkine, and A. Revcolevschi, Phys. Rev. B **62**, R6108 (2000).
[29] G. Simutis, S. Gvasaliya, N. S. Beesetty, T. Yoshida, J. Robert, S. Petit, A. I. Kolesnikov, M. B. Stone, F. Bourdarot, H. C. Walker, D. T. Adroja, O. Sobolev, C. Hess, T. Masuda, A. Revcolevschi, B. Buchner, and A. Zheludev, Phys. Rev. B **95**, 054409 (2017).
[30] G. M. Sheldrick, Acta Crystallogr., Sect. A **64**, 112 (2008).
[31] B. H. Toby and R. B. Von Dreele, J. Appl. Crystallogr. **46**, 544 (2013).
[32] G. Kresse and J. Furthmüller, Phys. Rev. B **54**, 11169 (1996).
[33] G. Kresse and J. Hafner, Phys. Rev. B **48**, 13115 (1993).
[34] C. Lane, J. W. Furness, I. G. Buda, Y. Zhang, R. S. Markiewicz, B. Barbiellini, J. Sun, and A. Bansil, Phys. Rev. B **98**, 125140 (2018).
[35] M. F. Hundley, J. D. Thompson, S. W. Cheong, Z. Fisk, and S. B. Oseroff, Physica C **158**, 102 (1989).
[36] M. E. Fisher, Am. J. Phys. **32**, 343 (1964).
[37] S. M. Disseler, Y. Chen, S. Yeo, G. Gasparovic, P. M. B. Piccoli, A. J. Schultz, Y. Qiu, Q. Huang, S. W. Cheong, and W. Ratcliff, Sci. Rep. **5**, 17771 (2015).
[38] S. R. White and I. Affleck, Phys. Rev. B **54**, 9862 (1996).
[39] J. Sun, A. Ruzsinszky, and J. P. Perdew, Phys. Rev. Lett. **115**, 036402 (2015).
[40] B. Vargas, E. Ramos, E. Perez-Gutierrez, J. C. Alonso, and D. Solis-Ibarra, J. Am. Chem. Soc. **139**, 9116 (2017).

[41] J. W. Furness, Y. Zhang, C. Lane, I. G. Buda, B. Barbiellini, R. S. Markiewicz, A. Bansil, and J. Sun, Commun. Phys. **1**, 11 (2018).
[42] J. C. Bonner and M. E. Fisher, Phys. Rev. **135**, A640 (1964).
[43] I. Umegaki, H. Tanaka, N. Kurita, T. Ono, M. Laver, C. Niedermayer, C. Ruegg, S. Ohira-Kawamura, K. Nakajima, and K. Kakurai, Phys. Rev. B **92**, 174412 (2015).
[44] S. Yamashita, T. Yamamoto, Y. Nakazawa, M. Tamura, and R. Kato, Nat. Commun. **2**, 1274 (2011).
[45] Y. Shen, Y.-D. Li, H. Wo, Y. Li, S. Shen, B. Pan, Q. Wang, H. C. Walker, P. Steffens, M. Boehm, Y. Hao, D. L. Quintero-Castro, L. W. Harriger, M. D. Frontzek, L. Hao, S. Meng, Q. Zhang, G. Chen, and J. Zhao, Nature (London) **540**, 559 (2016).
[46] H. K. Collan, M. Krusius, and G. R. Pickett, Phys. Rev. B **1**, 2888 (1970).
[47] T. Chakrabarty, I. Heinmaa, V. Y. Verchenko, P. L. Paulose, and R. Stern, Phys. Rev. B **100**, 094431 (2019).
[48] J. Schlappa, U. Kumar, K. J. Zhou, S. Singh, M. Mourigal, V. N. Strocov, A. Revcolevschi, L. Patthey, H. M. Roennow, S. Johnston, and T. Schmitt, Nat. Commun. **9**, 5394 (2018).
[49] A. A. Belik, M. Azuma, and M. Takano, J. Solid State Chem. **177**, 883 (2004).
[50] A. A. Belik, M. Azuma, and M. Takano, Inorg. Chem. **44**, 7523 (2005).
[51] I. Tsukada, J. Takeya, T. Masuda, and K. Uchinokura, Phys. Rev. B **62**, R6061 (2000).
[52] V. A. Pashchenko, A. Sulpice, F. Mila, P. Millet, A. Stepanov, and P. Wyder, Eur. Phys. J. B **21**, 473 (2001).
[53] J. M. Law, C. Hoch, R. Glaum, I. Heinmaa, R. Stern, J. Kang, C. Lee, M. H. Whangbo, and R. K. Kremer, Phys. Rev. B **83**, 180414(R) (2011).
[54] R. Ruckamp, J. Baier, M. Kriener, M. W. Haverkort, T. Lorenz, G. S. Uhrig, L. Jongen, A. Moller, G. Meyer, and M. Gruninger, Phys. Rev. Lett. **95**, 097203 (2005).
[55] A. Seidel, C. A. Marianetti, F. C. Chou, G. Ceder, and P. A. Lee, Phys. Rev. B **67**, 020405(R) (2003).
[56] B. Lake, D. A. Tennant, C. D. Frost, and S. E. Nagler, Nat. Mater. **4**, 329 (2005).
[57] M. Kato, A. Hatazaki, K. Yoshimura, and K. Kosuge, Physica B **281**, 663 (2000).
[58] M. G. Banks, R. K. Kremer, C. Hoch, A. Simon, B. Ouladdiaf, J. M. Broto, H. Rakoto, C. Lee, and M. H. Whangbo, Phys. Rev. B **80**, 024404 (2009).
[59] M. Baenitz, C. Geibel, M. Dischner, G. Sparn, F. Steglich, H. H. Otto, M. Meibohm, and A. A. Gippius, Phys. Rev. B **62**, 12201 (2000).
[60] R. L. Carlin, R. Burriel, F. Palacio, R. A. Carlin, S. F. Keij, and D. W. Carnegie, Jr., J. Appl. Phys. **57**, 3351 (1985).
[61] T. L. Bergman and F. P. Incropera, *Introduction to Heat Transfer* (Wiley, Hoboken, NJ, 2011).
[62] J. Calloway, Phys. Rev. **113**, 1046 (1959).
[63] J. Jacques des Cloizeaux and J. Pearson, Phys. Rev. **128**, 2131 (1962).